Mathematical Technique for Predicting Thermal Exchange Dynamics in the Circulatory System

[1] Salihu, N. O., [2] R. O. Olayiwola, and [3] Salihu A. O
[1,2] Department of Mathematics, Federal University of Technology, Minna, Niger State, Nigeria.
[3] Department of Science and Laboratory Technology, School of Applied Sciences, Kogi State Polytecchnic, Lokoja, Nigeria
[1*] Corresponding author email: so.nasiru@futminna.edu.ng

Abstract

Mathematical methods were employed to study and forecast heat transfer patterns that occur in the human circulatory system. The research establishes a blood flow model which treats blood as a Newtonian fluid that flows through a porous medium while its viscosity changes with hematocrit levels. The research assumes that thermal conductivity shows temperature-dependent behavior. The study uses the parameter expansion method together with the eigenfunction technique to solve the governing equations which describe the fluid flow and thermal interactions. The research presents analytical solutions which explain both blood flow velocity distribution and temperature distribution throughout blood and adjacent tissue. The research uses Computer Symbolic Algebra system MAPLE 17 as its computational tool and displays the results through graphical representations which help users understand the data. The study demonstrates that velocity profiles depend on multiple factors which include hematocrit level magnetic field strength permeability Reynolds number and pressure gradient. Temperature changes in tissue and blood result from three key elements which include Peclet number pressure gradient and perfusion rate. The results show that the flow velocity achieves its maximum value at $\phi(\eta,t)=3.1$ when $\eta=0$ while blood temperature attained maximum values when $\eta=0$ and $t=0.5$. The research revealed that the blood flow velocity tends to zero $\left(\phi(\eta,t)\to 0\right)$ as the Hartmann number varies from 0 to 4.0. This implies that the strength of Lorentz force produced become stronger with an increase in Hartmann number that leads to retardation on the blood's motion and this indicates that to ensure the flow along the artery region is properly controlled, a certain strength of magnetic intensity is required. The research also revealed that at a temperature ratio, $\left(\alpha=0\right)$ the blood temperature was minimal while the temperature ratio $\left(\alpha=-1.0,\ \alpha=1.0\right)$ resulted in a maximal high blood temperature.

Keywords: Circulatory System, Hartmann Number, Magnetic Field, Temperature, Thermal Exchange, Velocity.

Introduction

The system consists of three main parts which include the heart that maintains blood flow and the blood vessel system which functions as transport channels and the blood which carries oxygen and nutrients and waste products throughout the body. The system functions through two pathways which work together as one system. The systemic circulation delivers oxygen-rich blood to all body organs and tissues while the pulmonary circulation enables gas exchange because it brings oxygen into the bloodstream and removes carbon dioxide from the body (Taura et al., 2024).

Biological systems demand precise blood flow analysis through mathematical models which need complete structure for their development. The analysis of these processes becomes difficult because they require analysis of both solid tissue components and liquid blood components (Bessonov et al., 2023). The development of thermal modeling for biological systems has progressed to include blood flow effects because researchers now understand blood flow functions as a heat transfer mechanism. Biological tissues transfer heat through conduction as their main mechanism because blood flows through narrow capillaries at a slow speed and this effect decreases blood flow through the body (Salihu, 2023).

The principles develop practical applications through their use in thermal medical treatments which employ thermal ablation to use heat for destroying abnormal tissue. The success of these procedures depends on how temperature distribution reaches its required level (Blyakhman et al., 2025). Blood flow within tissues typically follows a path from arteries through capillaries to veins. The body needs to establish separate energy balance equations which will explain blood movement through larger vessels because thermal equilibrium between blood and surrounding tissue does not occur (Buchanan et al., 2000).

Blood circulation creates a major obstacle which inhibits the success of thermal treatments because it produces a cooling impact. Flowing blood can remove heat from the treatment region, reducing the effectiveness of the applied thermal dose. Treatment design and analysis requires treatment designers to carefully assess this heat loss mechanism (Shih et al., 2025).

Researchers have conducted multiple studies to forecast temperature distribution in perfused tissues while creating models that fulfill essential physical and biological criteria. The system must follow energy conservation laws while generating heat transfer calculations which show blood and tissue heat movement without requiring blood vessel tracking and it must function for both heated and unheated tissue states (Shit and Roy, 2023). In order to attain these objectives, researchers have come up with a number of mathematical models simplifying the complex interactions of vascularized tissues and yet, are physically accurate. The purpose of this study is to use mathematical methods to study and forecast thermal exchange in the circulatory system including the influence of pulsatile blood flow and time-dependent thermal conductivity.

Mathematical Formulation

The current analysis takes into account a pulsatile blood flow through a vessel under a set of assumptions. It is supposed that the vessel is straight with rigid and porous walls, and the blood is assumed to be a laminar, incompressible and a Newtonian fluid. In these assumptions, the equations of temperature distribution in the surrounding tissue and thermal energy transport in blood are developed according to the existing models, which are found in the literature (Zhang et al., 2025; Blyakhman et al., 2025). These equations model the interaction between the fluid motion and the heat transfer and can be used to analyze the process of thermal exchange in the circulatory system as:

$$\rho_t c_t \frac{\partial T_t}{\partial t} = \left(\frac{1}{r} \frac{\partial}{\partial r} \left(k_t r \frac{\partial T_t}{\partial r} \right) + \frac{\partial}{\partial z} \left(k_t \frac{\partial T_t}{\partial z} \right) \right) - W_b c_b \left(T_t - T_a \right) + Q_t \left(r, z, t \right) \tag{1}$$

$$\rho_b c_b \left(\frac{\partial T_b}{\partial t} + w \frac{\partial T_b}{\partial z} \right) = \left(\frac{1}{r} \frac{\partial}{\partial r} \left(k_b r \frac{\partial T_b}{\partial r} \right) + \frac{\partial}{\partial z} \left(k_b \frac{\partial T_b}{\partial z} \right) \right) + Q_b \left(r, z, t \right) \tag{2}$$

$$Q_t(r,z,t) = Q_{t_0}\frac{\pi}{2}\sin\left(\frac{\pi_t}{t_h}\right) \tag{3}$$

$$Q_b(r,z,t) = Q_{b_0}\frac{\pi}{2}\sin\left(\frac{\pi_t}{t_h}\right) \tag{4}$$

$$\rho\frac{\partial w}{\partial t} = -\frac{\partial p}{\partial z} + \frac{1}{r}\frac{\partial}{\partial r}\left(r\mu(r)\frac{\partial w}{\partial r}\right) - \sigma B_0^2 w - \frac{\mu(r)}{\bar{k}}w \tag{5}$$

$$\mu(r) = \mu_0(1+\beta h(r)) \quad \text{(Shih } et\ al.,\ 2025) \tag{6}$$

$$h(r) = H\left(1-\left(\frac{r}{R_0}\right)^m\right) \quad \text{(Shih } et\ al.,\ 2025) \tag{7}$$

The initial and boundary conditions are formulated as

$$\left\{\begin{array}{l} w(r,z,0)=0, \left.\dfrac{\partial w}{\partial r}\right|_{r=0}=0, w(R_0,z,t)=0 \\ T_t(r,z,0)=T_a, \left.\dfrac{\partial T_t}{\partial r}\right|_{r=0}=0, T_t(R_0,z,t)=T_a \\ T_b(r,z,0)=T_a, \left.\dfrac{\partial T_b}{\partial r}\right|_{r=0}=0, T_b(R_0,z,t)=T_a \end{array}\right\} \tag{8}$$

In this study, $z$represents the axial coordinate along the length of the vessel, while $r$denotes the radial position measured from the center of the vessel. The symbol ρrefers to the density of blood, and $w$is the axial velocity of blood flow, with $w_0$indicating its initial value. The variable $p$corresponds to blood pressure. The viscosity of blood, which varies with radial position, is expressed as $\mu(r)$. Similarly, the hematocrit distribution is represented by $h(r)$, where Hdenotes the maximum hematocrit value at the կենտրոն of the artery. The parameter $\mu_0$defines the viscosity coefficient of plasma. The radius of a normal arterial segment is given by R_0, while $\beta$is a constant parameter for blood, typically taken as 2.5. Electrical conductivity is denoted by σ, and B_0represents the strength of the externally applied magnetic field. The permeability of the porous medium is described by k. Thermal conductivity is distinguished for tissue and blood, represented by $k_t$and k_b, respectively. Likewise, the specific heat capacities are given by $c_t$for tissue and $c_b$for blood. Temperature variables include $T_t$for tissue temperature and $T_b$for blood temperature, while the ambient temperature is denoted by T_a, which is commonly assumed to be $37°C$. The parameter $w_b$represents the perfusion mass flow rate. Heat generation within the system is described by $Q_t(r,z,t)$, which accounts for heat added to the tissue in an axisymmetric manner, and $Q_b(r,z,t)$, which represents the corresponding heat addition in the blood. Finally, Ldenotes the length of the blood vessel segment under consideration. Equations (1) to (8) are transformed in Cartesian coordinates $(r,r\theta,z)\to(x,y,z)$ and $(u_r,u_\theta,u_z)\to(u,v,w)$ to become

$$\rho_t c_t\frac{\partial T_t}{\partial t} = \frac{\partial}{\partial x}\left(k_t\frac{\partial T_t}{\partial x}\right) + \frac{\partial}{\partial z}\left(k_t\frac{\partial T_t}{\partial z}\right) - w_b c_b(T_t - T_a) + Q_t(x,z,t) \tag{9}$$

$$\rho_b c_b\left(\frac{\partial T_b}{\partial t}+w\frac{\partial T_b}{\partial z}\right)=\frac{\partial}{\partial x}\left(k_b\frac{\partial T_b}{\partial x}\right)+\frac{\partial}{\partial z}\left(k_b\frac{\partial T_b}{\partial z}\right)+Q_b(x,z,t) \tag{10}$$

Where,

$$k_t=k_{t_0}\left(\frac{T_t}{T_a}\right) \tag{11}$$

$$k_b=k_{b_0}\left(\frac{T_b}{T_a}\right) \tag{12}$$

$$\rho\frac{\partial w}{\partial t}=-\frac{\partial p}{\partial z}+\frac{\partial}{\partial x}\left(\mu(x)\frac{\partial w}{\partial x}\right)-\sigma B_0^2 w-\frac{\mu(x)}{k}w \tag{13}$$

Where,

$$u(x)=\mu_0(1+\beta h(x)) \tag{14}$$

$$h(x)=H\left(1-\left(\frac{x}{R_0}\right)^m\right) \tag{15}$$

With initial and boundary conditions:

$$\left\{\begin{array}{l} w(x,z,0)=0,\ \left.\frac{\partial w}{\partial x}\right|_{x=0}=0,\ w(R_0,z,t)=0 \\ T_t(x,z,0)=T_a,\ \left.\frac{\partial T_t}{\partial x}\right|_{x=0}=0,\ T_t(R_0,z,t)=T_a \\ T_b(x,z,0)=T_a,\ \left.\frac{\partial T_b}{\partial x}\right|_{x=0}=0,\ T_b(R_0,z,t)=T_a \end{array}\right\} \tag{16}$$

A new space variable was introduced as:

$$\varepsilon=x+z \tag{17}$$

Solving equations (9) to (17) with equation (17), we have

$$\rho\frac{\partial w}{\partial t}=-\frac{\partial p}{\partial \varepsilon}+\frac{\partial}{\partial \varepsilon}\left(\mu(\varepsilon)\frac{\partial w}{\partial \varepsilon}\right)-\sigma B_0^2 w-\frac{\mu(\varepsilon)}{k}w \tag{18}$$

$$\rho_t c_t \frac{\partial T_t}{\partial t} = 2\frac{\partial}{\partial \varepsilon}\left(k_t \frac{\partial T_t}{\partial \varepsilon}\right) - w_b c_b \left(T_t - T_a\right) + Q_t\left(\varepsilon, t\right) \tag{19}$$

$$\rho_b c_b \left(\frac{\partial T_b}{\partial t} + w\frac{\partial T_b}{\partial \varepsilon}\right) = 2\frac{\partial}{\partial \varepsilon}\left(k_b \frac{\partial T_b}{\partial \varepsilon}\right) + Q_b\left(\varepsilon, t\right) \tag{20}$$

Where,

$$\mu(\varepsilon) = \mu_0\left(1 + \beta H\left(1 - \left(\frac{\varepsilon}{R_0}\right)^m\right)\right) \tag{21}$$

With initial and boundary conditions:

$$\left\{\begin{array}{l} w\left(\varepsilon,0\right) = 0,\ \left.\dfrac{\partial w}{\partial \varepsilon}\right|_{\varepsilon=0} = 0,\ w\left(R_0,t\right) = 0 \\ T_t\left(\varepsilon,0\right) = T_a,\ \left.\dfrac{\partial T_t}{\partial \varepsilon}\right|_{\varepsilon=0} = 0,\ T_t\left(R_0,t\right) = T_a \\ T_b\left(\varepsilon,0\right) = T_a,\ \left.\dfrac{\partial T_b}{\partial \varepsilon}\right|_{\varepsilon=0} = 0,\ T_b\left(R_0,t\right) = T_a \end{array}\right\} \tag{22}$$

We non – dimensionalize equations (18) – (22) using the following dimensionless variables:

$$\left\{\begin{array}{l} \eta = \dfrac{\varepsilon}{R_0},\ \tau = \dfrac{w_0 t}{R_0},\ \phi = \dfrac{w}{w_0},\ \alpha = \dfrac{T_b}{T_t} \\ \theta = \dfrac{T_t - T_a}{\alpha T_a},\ \psi = \dfrac{T_b - T_a}{\alpha T_a},\ p' = \dfrac{p}{\rho w_0^2} \end{array}\right\} \tag{23}$$

Then equation (18) to (22) becomes

$$\frac{\partial \phi}{\partial \tau} = -\frac{\partial p'}{\partial \eta} + \frac{1}{\mathrm{Re}}\frac{\partial}{\partial \eta}\left(\left(1 + \beta H\left(1 - \eta^m\right)\right)\frac{\partial \phi}{\partial \eta}\right) - M\phi - k_p\left(\left(1 + \beta H\left(1 - \eta^m\right)\right)\phi\right) \tag{24}$$

$$\frac{\partial \theta}{\partial \tau} = \lambda_1 \frac{\partial}{\partial \eta}\left(\left(1 + \alpha\theta\right)\frac{\partial \theta}{\partial \eta}\right) - \alpha_1\theta + \gamma_1 \sin\left(\frac{\pi_t}{t_h}\right) \tag{25}$$

$$\frac{\partial \psi}{\partial \tau} + \phi\frac{\partial \psi}{\partial \eta} = \lambda_2 \frac{\partial}{\partial \eta}\left(\left(1 + \alpha\theta\right)\frac{\partial \psi}{\partial \eta}\right) + \gamma_2 \sin\left(\frac{\pi_t}{t_h}\right) \tag{26}$$

$$\left\{\begin{array}{l}\phi(\eta,0)=0,\quad \left.\dfrac{\partial\phi}{\partial\eta}\right|_{\eta=0}=0,\quad \phi(1,\tau)=0\\ \theta(\eta,0)=0,\quad \left.\dfrac{\partial\theta}{\partial\eta}\right|_{\eta=0}=0,\quad \theta(1,\tau)=0\\ \psi(\eta,0)=0,\quad \left.\dfrac{\partial\psi}{\partial\eta}\right|_{\eta=0}=0,\quad \psi(1,\tau)=0\end{array}\right\} \tag{27}$$

Method of Solution

When $\dfrac{\partial p'}{\partial\eta}=f=$ constant, $\mu=$ constant, $k_t=$ constant, and $k_b=$ constant. Then equations (24) - (27) reduce to:

$$\frac{\partial\phi}{\partial\tau}=-f+\frac{1}{\mathrm{Re}}\frac{\partial^2\phi}{\partial\eta^2}-M\phi-k_p\phi \tag{28}$$

$$\frac{\partial\theta}{\partial\tau}=\lambda_1\frac{\partial^2\theta}{\partial\eta^2}-\alpha_1\theta+\gamma_1 Sin\left(\frac{\pi_t}{t_h}\right) \tag{29}$$

$$\frac{\partial\psi}{\partial\tau}+b\beta\phi\frac{\partial\psi}{\partial\eta}=\lambda_2\frac{\partial^2\psi}{\partial\eta^2}+\gamma_2 Sin\left(\frac{\pi_t}{t_h}\right) \tag{30}$$

Where

$$b=\frac{1}{\beta} \tag{31}$$

We solve equations (28) - (30) with their initial and boundary conditions in equation (27) using parameter expansion method and eigenfunction technique as follows,

Let $0<\beta\le 1$, and suppose the solution of the equations (28) - (30) can be given as;

$$\left\{\begin{array}{l}\phi=\phi_0+\beta\phi_1+\ldots\\ \theta=\theta_0+\beta\theta_1+\ldots\\ \psi=\psi_0+\beta\psi_1+\ldots\end{array}\right\} \tag{32}$$

Using equation (32) in equations (28) - (30), then, equations (28) - (30) can be approximated as

$$\frac{\partial}{\partial\tau}(\phi_0+\beta\phi_1+\ldots)=-fe^{-\sigma t}+\frac{1}{\mathrm{Re}}\frac{\partial^2}{\partial\eta^2}(\phi_0+\beta\phi_1+\ldots)-(M+k_p)(\phi_0+\beta\phi_1+\ldots) \tag{33}$$

$$\frac{\partial}{\partial\tau}(\theta_0+\beta\theta_1+\ldots)=\lambda_1\frac{\partial^2}{\partial\eta^2}(\theta_0+\beta\theta_1+\ldots)-\alpha_1(\theta_0+\beta\theta_1+\ldots)+\gamma_1 Sin\left(\frac{\pi_t}{t_h}\right) \tag{34}$$

$$\frac{\partial}{\partial\tau}(\psi_0+\beta\psi_1+...)+b\beta(\phi_0+\beta\phi_1+...)\frac{\partial}{\partial\eta}(\psi_0+\beta+\psi_1+...)=\begin{pmatrix}\lambda_2\frac{\partial^2}{\partial\eta^2}(\psi_0+\beta\psi_1+...)+\\ \gamma_2 Sin\left(\frac{\pi_t}{t_h}\right)\end{pmatrix} \quad (35)$$

Where,

$$b=\frac{1}{\beta} \quad (36)$$

Collecting like powers of β, with further operation gives:

$$\theta_0(\eta,t)=U_0(t)+\sum_{n=1}^{\infty}U_n(t)CosA\eta \quad (37)$$

Where

$$U_0(t)=2S_1\int_0^t e^{-\alpha_1(t-\tau)}d\tau\ =\frac{2S_1}{\alpha_1}\left(1-e^{-\alpha_1 t}\right) \quad (38)$$

$$U_n(t)=\int_0^t e^{-\left(\alpha_1+\lambda_1A^2\right)(t-\tau)}\left(\frac{2S_1(-1)^{n+1}}{A}\right)d\tau+0e^{-\left(\alpha_1+\lambda_1A^2\right)t} \quad (39)$$

$$=\frac{2S_1(-1)^{n+1}\left(1-e^{-\left(\alpha_1+\lambda_1A^2\right)t}\right)}{A\left(\alpha_1+\lambda_1A^2\right)} \quad (40)$$

Also,

$$\psi_0(\eta,t)=U_0(t)+\sum_{n=0}^{\infty}U_n(t)CosA\eta \quad (41)$$

Where

$$U_0(t)=\int_0^t e^{0(t-\tau)}2S_2d\tau+0e^{0t} \quad (42)$$

$$2S_2\int_0^t d\tau=2S_2t \quad (43)$$

$$U_n(t)=\int_0^t e^{-\lambda_2A^2(t-\tau)}\left(\frac{2S_2(-1)^{n+1}}{A}\right)d\tau+0e^{-\lambda_2A^2(t-\tau)} \quad (44)$$

$$=\frac{2S_2(-1)^{n+1}}{\lambda_2A^3}\left(1-e^{-\lambda_2A^2t}\right) \quad (45)$$

And

$$\phi_1(\eta,t) = 0 + \sum_{n=0}^{\infty}(0)CosA\eta = 0 \tag{46}$$

Where

$$U_0(t) = \int_0^t e^{-(\delta_1+\delta_3 A^2)(t-\tau)}\left(\frac{2(-1)^n f}{A}\right)d\tau + 0e^{-(\delta_1+\delta_3 A^2)t} \tag{47}$$

$$U_n(t) = \frac{2(-1)^n f\left(1-e^{-(\delta_1+\delta_3 A^2)t}\right)}{A\left(\delta_1+\delta_3 A^2\right)} \tag{48}$$

Results and Discussions

To better illustrate the application of the proposed mathematical approach for analyzing thermal exchange in the circulatory system, the results are presented in graphical form using MAPLE computational software. These graphical representations help to clearly show how different physical parameters influence the behavior of blood flow and heat transfer within the system.

The study examines the impact of key parameters on three major aspects: flow velocity, temperature distribution in the tissue, and temperature variation in the blood. Special attention is given to models that account for changes in blood viscosity due to hematocrit levels, as well as variations in thermal conductivity with temperature. The graphical results provide useful insights into how these factors interact and affect both fluid motion and thermal behavior in biological tissues.

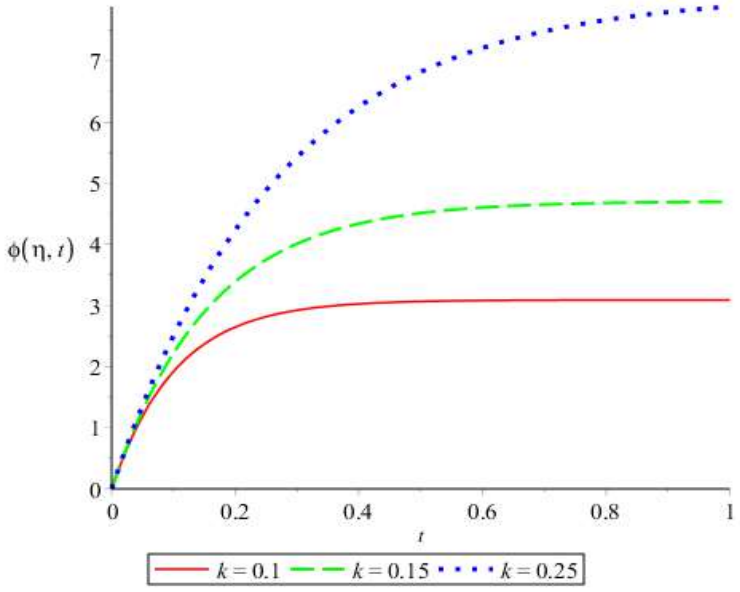

Figure 1: Graph of velocity against time for different values of permeability parameter

Figure 1 shows the graph of velocity profile $\phi(\eta,t)$ for different values of permeability parameter (k). It is observed that velocity increase and later became steady with time and maximum velocity increases as value permeability parameter increases.

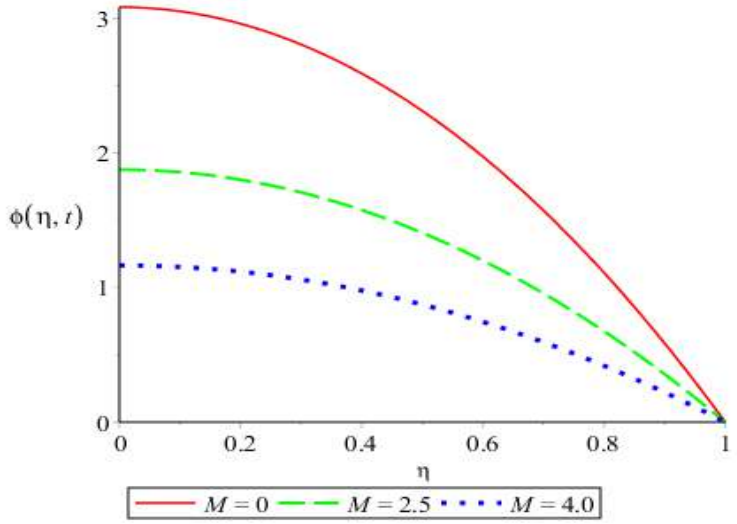

Figure 2: Graph of velocity against distance for different values of Hartmann number

Figure 2 displays the graph of velocity profile $\phi(\eta,t)$ for different values of Hartmann number (M). It is observed that velocity decreases along the distance and this velocity decreases as Hartmann number increases.

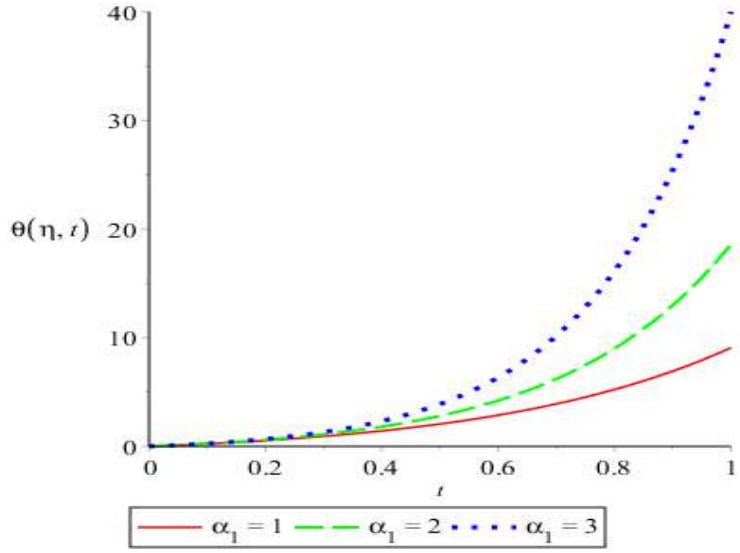

Figure 3: Graph of tissue temperature against time for different values of perfusion mass flow rate.

Figure 3 depicts the graph of tissue temperature profile $\theta(\eta,t)$ for different perfusion mass flow rate (α_1). It is observed that tissue temperature increase with time and maximum temperature increases as perfusion mass flow rate increases.

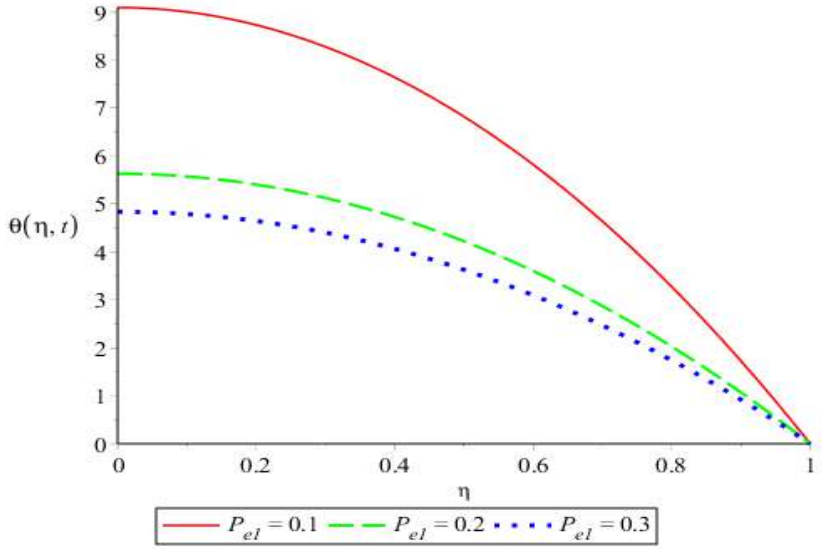

Figure 4: Graph of tissue temperature against distance for different values of Peclet number

Figure 4 shows the graph of tissue temperature profile $\theta(\eta,t)$ for different values of Peclet number (P_{el}). It is observed that tissue temperature decreases along the distance and this temperature increases as Peclet number increases.

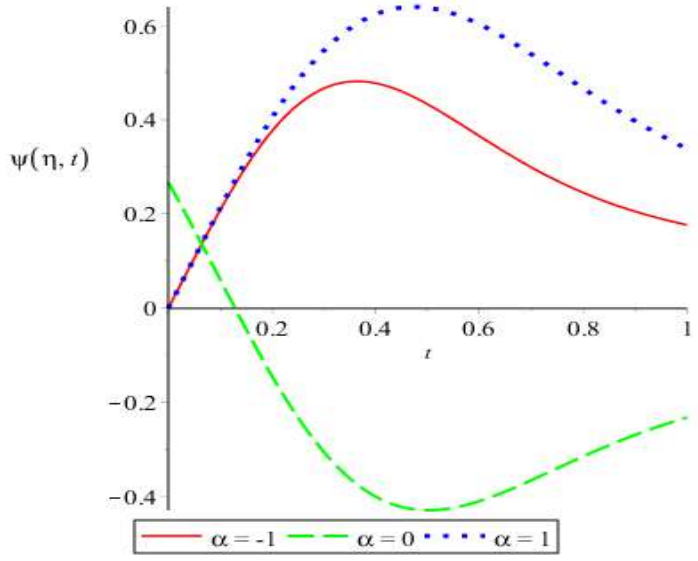

Figure 5: Graph of blood temperature against time for different values of temperatures ratio.

Figure 5 depicts the graph of blood temperature profile $\psi(\eta,t)$ against time for different values of temperature ratio (α). It is observed that we have positive blood temperature profile when $\alpha<0$ and $\alpha>0$ while we have negative blood temperature profile when $\alpha=0$. This by implication means that variable thermal conductivity bring about increase in blood temperature.

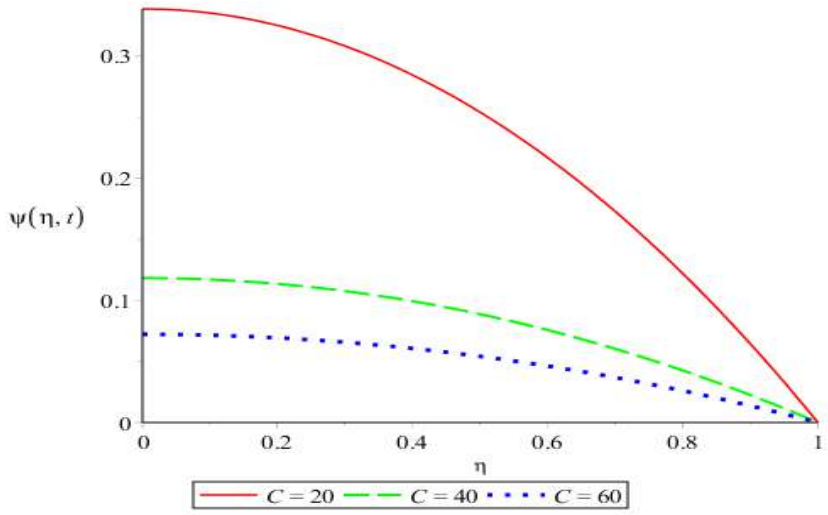

Figure 6: Graph of blood temperature against distance for different values of pressure gradient parameter

Figure 6 shows the graph of blood temperature profile $\psi(\eta,t)$ for different values of pressure gradient parameter (C). It is observed that blood temperature decreases along the distance and this temperature decreases as values of pressure gradient increases.

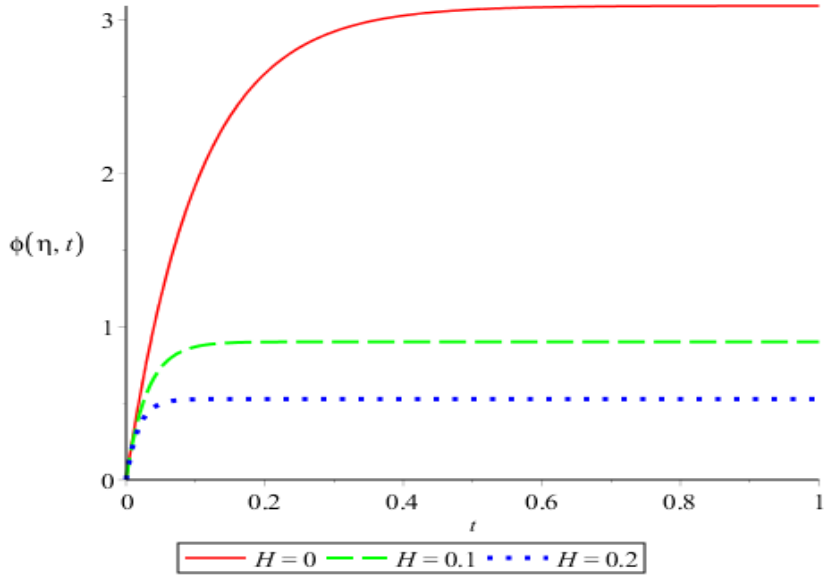

Figure 7: Graph of velocity against time for different values of hematocrit

Figure 7 shows the graph of velocity profile $\phi(\eta,t)$ for different values of hematocrit (H). It is observed that velocity increase and later became steady with time and maximum velocity decreases as values of hematocrit increases.

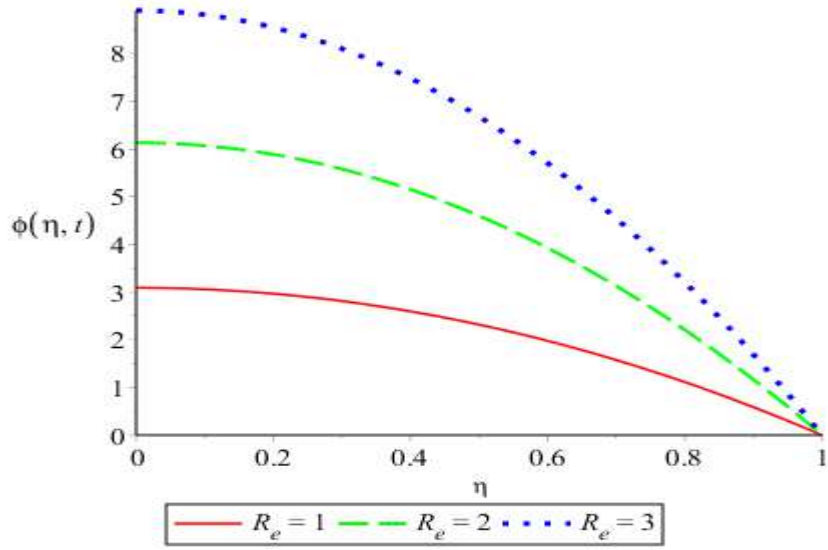

Figure 8: Graph of velocity against distance for different values of Reynolds number

Figure 8 displays the graph of velocity profile $\phi(\eta,t)$ for different values of Reynolds number (R_e). It is observed that velocity decreases along the distance and this velocity increases as Reynolds number increases.

Conclusion

This work presents a theoretical investigation into the mechanisms governing heat transfer and fluid flow within the circulatory system under the influence of a magnetic field. The analysis incorporates important physiological factors, including the dependence of blood viscosity on hematocrit and the variation of thermal conductivity with temperature. The governing equations were solved analytically using the parameter expansion method together with the eigenfunction technique.

From the analysis, several important observations can be made:

- An increase in blood thermal conductivity leads to a rise in blood temperature.
- Higher perfusion rates contribute to an increase in tissue temperature.
- A stronger pressure gradient accelerates blood flow but tends to lower blood temperature.
- Increased hematocrit levels result in a reduction in flow velocity.
- The presence of a magnetic field (Hartmann effect) suppresses blood flow velocity.
- Both Reynolds number and permeability of the medium promote an increase in flow velocity.
- Higher Peclet numbers lead to a decrease in both tissue and blood temperatures.

Overall, the study highlights the combined effects of physiological and physical parameters on heat transfer and blood flow, providing useful insights that may be relevant in biomedical applications such as thermal therapies and treatment planning.

References

Salihu O. N. (2023). Effects of Pollutants and Atmospheri Temperature Rise on Agriculture. *Journal of the Nigerian Association of Mathematical Physics,* 35, 115 – 124.

Bessonov, N., Sequeira, A., Simakov, S., Vassilevskii, Y., & Volpert, V. (2023). Method of Blood Flow Modeling. *Journal of Math. Model Nat. Phenom.,* 11(1), 1-25.

Blyakhman, F., Buznikov, N., Sklyar, T., Safronov, A., Golubeva, E., Svalov, A., & Kurlyandskaya, G. (2025). Mechanical, Electrical and Magnetic Properties of Ferrogels with Embedded Iron Oxide Nanoparticles Obtained by Laser Target Evaporation: Focus on Multifunctional Biosensor Applications. *Sensors* 2018, 18, 872.

Buchanan, J. R., Kleinstreuer, C. & Corner, J. K. (2000). Rheological effects on pulsatile hemodynamic in a stenosed tube, *Computers& Fluids,*29 (4), 695–724.

Shih, T. C., Kou, H. S., & Lin, W. L. (2025). Cooling Effect of Thermally Significant Blood Vessel in Perfused Tumor Tissue During Thermal Therapy. *International Commune Heat Mass,* 33, 135 – 141.

Shit, G. C., & Roy, M. (2023). Pulsatile flow and heat transfer of a magneto micropolar fluid through a stenosed artery under the influence of body acceleration, *Journal of Mechanics in Medicine and Biology,* 11 (5), 643–661.

Taura, L. S., Ishiyaku, I. B., & Kawo, A. H. (2024). The use of continuity equation of fluid mechanics to reduce the abnormality of the cardiovascular system: A control mechanics of the human heart. *Journal of Biophysics and Structural Biology,* 4(1), 1-12.

Urquiza, S. A., Blanco, P. J., Venere, M. J., & Feijoo, R. A. (2024). Multidimensional Modeling for the Carotid Artery Blood Flow. *Elsevier Science Direct*, 45, 131 – 149.

Zhang, Q., Sun, Y., & Yang, J. (2025). Bio-heat transfer analysis based on fractional derivative and memory-dependent derivative heat conduction models. Case Study. *Therm. Eng*., 27, 101 - 211.